Experimental Investigation of Heat Transfer and Second Law Analysis in a Pebble Bed Channel with Internal Heat Generation

Published in:
International Journal of Heat and Mass Transfer

Document Version:
Publisher's PDF, also known as Version of record

Queen's University Belfast - Research Portal:
Link to publication record in Queen's University Belfast Research Portal

Experimental investigation of heat transfer and second law analysis in a pebble bed channel with internal heat generation

CrossMark

Meysam Nazari [a], Davood Jalali Vahid [a], Rahim Khoshbakhti Saray [a], Yasser Mahmoudi [b,*]

[a] Department of Mechanical Engineering, Sahand University of Technology, Tabriz, Iran
[b] School of Mechanical and Aerospace Engineering, Queen's University Belfast, Belfast BT9 5AH, UK

ABSTRACT

This paper studies experimentally the forced convection heat transfer of turbulent flow in a cylindrical pebble bed channel with internal heat generation. Exergy and entropy generation analyses are performed to optimize energy conversion in the system identify the destruction of exergy in the pebble bed channel. Stainless steel spheres are used in stacked pebble bed channel. Internal heating is generated uniformly by electromagnetic induction heating method in metallic spheres. Dry air is used as the working fluid in the process of cooling of the heated spheres. The experiment is performed for turbulent flow regimes with Reynolds (Re_d) number (based on the diameter of the spheres) in the range of 920–2570, which is equal to Reynolds (Re) number, based on channel diameter, in the range of 4500–10,000. The effects of different parameters, including spheres diameter (d = 5.5, 6.5 and 7.5 mm), inlet volumetric flow rate ($\dot{V}$) and internal heat generation (Q) on the forced convection heat transfer, exergy transfer and entropy generation are studied. For second law and exergy analyses, mean exergy transfer Nusselt number (Nu_e) and entropy generation number (N_s) are investigated. Results show that for a fixed d and Q, the mean exergy transfer Nusselt number (Nu_e) decreases with the increase of Re_d number until it becomes zero for a critical Re_d number. This critical Re_d number found to be about 1450, 1800 and 2300 for d = 5.5, 6.5 and 7.5 mm, respectively. Further increase in the Re_d number, decreases Nu_e to negative values. It is found for spheres with diameter of d = 5.5 mm and for a fixed Q, as Re_d increases, the entropy generation number N_s increases monotonically. While, for d > 5.5 mm and fixed Q, the entropy generation number (N_s) decreases with the increase of Re_d number up to a critical Re_d value that makes N_s to be minimum. Further increase in Re_d number, increases N_s. It is also found that for Re_d > 1800, among the sphere diameters studied in this work, balls with highest diameters yield the minimum entropy generation in the system.

1. Introduction

Currently, nuclear energy is an important part of the energy mix, which generates roughly 10% of the world's electricity, making up around one-third of the world's low-carbon electricity supply [1]. Pebble-bed reactor (PBR) is a type of very-high-temperature reactor (VHTR) one of the six classes of nuclear reactors (e.g. [2,3]). The basic design of pebble-bed reactors features spherical uranium spheres as fuel called pebbles, which create a reactor core and are cooled by a gas such as helium, nitrogen or carbon dioxide that does not react chemically with the fuel elements [2]. The coolant circulates through the spaces between the fuel pebbles to carry heat away from the reactor. Ideally, the heated gas is run directly through a turbine to produce electrical power and industrial process heat applications [2].

The core of the pebble bed reactor can be considered as a fixed or packed bed (e.g. [4,5]). Packed bed reactor design is based upon the mechanisms of heat and mass transfer and the flow and pressure drop of the fluid through the bed of solids. The capability of removing the heat produced in the core is a key point of safety and reliability of the pebble bed reactor (e.g. [6]). To transfer the heat generated by nuclear fission reaction, the coolant enters this packed porous bed at the top and flows down through the voids between the hot fuel spheres, after which it leave the core at the bottom having been heated to a higher temperature (e.g. [4,7,8]). To calculate flow and heat transfer inside pebble beds and packed beds, the porous media approach is commonly used, in which a set of averaged equations is solved for a homogenized model of the pebble bed, using properties to describe the pebble packing (e.g. [4,7]). Present work focuses on the core of a packed bed reactor by analyzing the heat transfer characteristics, entropy generation and exergy destruction in a packed porous bed.

Nomenclature

A	contact surface area [m^2]		U	uncertainty
c_p	fluid specific heat [J/(kg K)]		u_D	Darcy velocity ($u_D = \varepsilon u$) [m/s]
D	channel diameter [m]		u	flow velocity [m/s]
d	spheres diameter [m]		$\dot{V}$	volumetric flow rate [m^3/s]
E	exergy transfer rate [W]		x	distance long the channel length [m]
$\acute{e}$	specific exergy [J/kg]			
f	friction factor			
h	heat transfer coefficient [W/m^2 K]		*Greek symbol*	
$\acute{h}$	specific enthalpy [J/kg]		ε	porosity
$\dot{I}$	irreversibility [W]		ρ	density [kg/m^3]
K	thermal conductivity [W/m K]		ϑ	specific volume [m^3/kg]
L	length of the channel [m]		ΔT	temperature difference [K]
MF	merit function		μ	dynamic viscosity [kg/m s]
$\dot{m}$	mass flow rate [kg/s]			
N	number of spheres			
Nu	Nusselt number		*Subscripts*	
N_s	entropy generation number		e	mean exergy
P	pressure [Pa]		ex	exergy
Pr	Prandtl number		0	environment
Q	generated heat [W]		f	fluid
Re	Reynolds number based on the channel diameter ($\mathrm{Re} = \rho u D/\mu$)		*gen*	generated
			in	inlet
Re$_d$	Reynolds number based on the spheres diameter ($\mathrm{Re} = \rho u d/\mu$)		*out*	outlet
			oi	outlet to inlet
St	Stanton number		q	energy transfer
s	specific entropy [J/kg K]		R	dependent variables
$\dot{s}$	entropy rate [W/K]		s	solid
T	temperature [K]		*sf*	solid to fluid
			V	independent variables
			x	local position

Studies regarding the heat transfer characteristics of flow in porous media are more concentrated on heat transfer enhancement in a channel or pipe subjected to a source of heat at the wall boundaries. In this regard, there were numerous experimental (e.g. [9–11]), theoretical (e.g. [12–18]) and numerical (e.g. [19–21]) studies in the past demonstrated the use of porous material as a promising passive technique in enhancing forced convection heat transfer in different industrial applications in micro and large scales. Heat transfer characteristics and enhancement in packed bed channels was also investigated by several researchers (e.g. [22–28]). Chrysler and Simons [29] investigated enhancement of convective heat transfer for removing heat from microelectronic chips using packed beds made of spherical particles. Izadpanah et al. [30] and Jamialahmadi et al. [31] studied single and two-phase flow forced convective heat transfer in a channel filled with metallic or non-metallic spherical particles under constant wall heat flux condition. They showed for single phase water flow that compared to an empty channel the rate of heat transfer increases about 2–4 times in the channel filled with a porous material. Forced convection heat transfer in a sintered and non-sintered porous media was studied experimentally by Jiang et al. [32,33] using water and air as working fluids under constant wall heat flux condition. For air as the working fluid and compared to the empty channel, they [32] fund that non sintered porous plate channel increases the rate of heat transfer by 4-8 times. They [33] also found that compared to non sintered porous media, sintered case is more efficient for increasing the rate of heat transfer.

The problem of internal heat generation on forced convection heat transfer in a channel or pipe filled with a porous material was investigated in a few studies. Bautista and Mendez [34] studied numerically the cooling process of a discrete heat source, which is placed in a rectangular-channel using a cooling fluid. The governing differential equation obtained in their study could predict the temperature variations of the heat source. In another study Atkhen and Berthoud [35] investigated experimentally the coolability in a volumetrically heated debris bed with water as the working fluid. They showed that coolant injection from the bottom of the system is at least two times more efficient than coolant injection from the top of the system. Single phase forced convection heat transfer of a water-cooled pebble bed reactor was investigated experimentally by Meng et al. [36] for a wide range of Reynolds number from 1000 to 8000, and stainless steel spheres with diameters of 3 and 8 mm. They used electromagnetic induction heating to generate heat in the porous channel filled with metal spheres. In their paper, the longitudinal and radial temperature distributions in porous media were discussed. They found that when the Re number increases, the heat transfer coefficient increases until it eventually stabilized. Smaller sphere diameters greatly improved the heat transfer. They also commented that the heating power had little effect on the heat transfer coefficient of the pebble bed channels, while it mainly affected the coolant temperature and physical parameters.

All the above mentioned studies, focused mainly on the generated heat, temperature distribution and pressure drop in the systems evolving porous medium, without analyzing the second law of thermodynamic. The work by Bejan [37] introduced the concept of entropy generation analysis due to fluid flow and heat transfer as a powerful tool to optimize variety of configurations when analyzing engineering problems. Since entropy generation destroys the work availability of a system, it makes good engineering sense to focus on irreversibility of heat transfer and fluid flow processes to understand the associated entropy generation mechanisms [38].

The second law analysis based on entropy generation was examined fundamentally for different thermal systems (e.g.

[37,39–41]). Although there are few analytical and numerical studies which were conducted to examine the entropy generation in the system containing porous materials (e.g. [42–44]), entropy generation and exergy destruction analysis of system containing porous materials are still developing. In addition, the experimental study of heat and fluid flow and entropy analysis of such systems are scarce. In this regard, Prommas et al. [45] experimentally studied the energy and exergy analyses in drying process of porous media using hot air. Experiments were conducted to find the effects of particle size and thermodynamics conditions on energy and exergy profiles.

Kurtbas et al. [46] studied experimentally the heat and exergy transfer characteristics of a forced convection flow through a horizontal rectangular channel where metal foams of different pore densities were placed. The bounding walls of the channel were subjected to uniform heat flux. They studied the use of porous material in enhancing heat transfer from the channel wall to the air flowing in the channel. Their experiments were conducted for various wall heat fluxes and a wide range of Reynolds number (based on channel height) from 600 to 33,000. Based on the exergy analysis they concluded that the mean exergy transfer Nusselt number decreases with the increase in Reynolds number and wall heat flux. Then, it becomes negative after definite value of the Reynolds number. However, in the experimental work of Kurtbas et al. [46] internal heat generation was not included.

A number of industrial applications involve internal heat generation such as nuclear reactor, agricultural product storage, electronic cooling, or a solar air heater packed with a porous medium, where the packed material provides the heat transfer enhancement and also acts as an absorbing media for the solar radiation [47]. It has been well demonstrated analytically by Yang and Vafai [12,48,49] and Vafai and Yang [50] that porous systems with internal heat generation can feature temperature gradient bifurcation. They showed that the internal heat generation in the solid phase is significant for the heat transfer characteristics. Meng et al. [36] studied experimentally heat transfer characteristics of pebble-bed channels with internal heat generation using water as the working fluid. The emphasis in their work was to obtain a holistic internal-heat-source pebble bed model based on the heat transfer. But, they did not performed entropy and or exergy analysis of the problem. Therefore, knowing the practical significance of entropy analysis and the role of internal heat generation in forced convection heat transfer in porous materials, the present work, aims at addressing this issue through an experimental study.

In the present work, we extend the work of Meng et al. [36] by performing both heat and exergy transfer analyses for a cylindrical pebble bed channel with internal heat generation, using air as the cooling working fluid. The channel is filled with steel spheres which are heated. We performed thermodynamic analysis to investigate heat and exergy transfer, and entropy generation of convective heat transfer in the porous channel for different flow parameters and steel sphere diameters. In real application, we study the problem of cooling a pebble bed cylindrical channel using air as the working fluid.

2. Experimental set-up

The experimental set-up is shown schematically in Fig. 1a and the real picture of the set-up is illustrated in Fig. 1b. The system comprises of a compressor, volumetric flow meter, test section, electrical power inputs, electromagnetic induction heating system and instrumentation to measure temperatures, pressures difference in the test section. The test section is a cylindrical channel made from Teflon material with an internal diameter of 27 mm, length of 133 mm and wall thickness of 16.5 mm. The Teflon

material and the thickness of the channel prevents heat loss from the test section to the ambient. This section was filled with packed steel spheres. The experiments were performed for three different numbers of steel balls (N) with different diameters (d), which give different porosity (ε) of the packed bed in the channel. These are (i) $d = 5.5$, $N = 473$, $\varepsilon = 0.45$ (ii) $d = 6.5$, $N = 290$, $\varepsilon = 0.46$ and (iii) $d = 7.5$, $N = 177$, $\varepsilon = 0.49$. In packed porous beds, side-wall effect causes a distribution of porosity across the channel and the near-wall positions have greater porosity. This distribution influences both the heat transfer and flow distribution. However, when the pebble diameter is small and the bed diameter is constant, as considered in this work, the side-wall effect is minimized [36]. The spheres inside the test section were supported by two perforated disks at the inlet and outlet of the test section [32]. Using electromagnetic induction technique, the steel spheres inside the test section were heated directly. The rate of generated heat inside the test section was controlled and varied between 54 W and 82 W by adjusting the input electric power.

Dry compressed air used as the working fluid in the heat transfer process inside the test section. As shown in Figs. 2a and 2b the local temperature of the air flow and metallic spheres porous media was measured by 10 (LM35 IC) temperature sensors. As shown schematically in Fig. 2b in order to measure the air temperature, 5 thermos sensors were inserted in the air flow near the wall of the test section. Furthermore, 5 sensors were embedded inside the test section to measure the local temperatures of the surface of heated spheres. These sensors were glued to the surface of spheres. The same approach was used by Nie et al. [51]. They [51] commented that this is to minimize the effect of flowing fluid on the thermos sensors. Although gluing the sensors may cause a delay in sensor response, but it can help to measure the solid surface temperature more accurately [51]. To measure the temperatures of the fluid at the inlet and outlet of the channel, 2 thermos sensors were separately located at the inlet and outlet of the test section. By making use of constant temperature oil bath, all of the thermos sensors were calibrated before installing. The measured temperatures were monitored by digital temperature indicators (SAMWON). The overall accuracy was within ±0.1 °C. The rate of input power to the test section was calculated by use of the voltage and current of the electromagnetic induction heating system, which were measured by digital multimeters. The pressure drop between the inlet and outlet of the test section was measured using U-type manometer. A rotameter type flow meter in the range of 100–200 lit/min was used to measure the flow rate of the injected air into the test section. Tests were carried out at different volumetric flow rates of air and power inputs. During each test, a constant power was supplied and the air volumetric flow rate was adjusted for a specified Reynolds number (defined based on the cylindrical channel diameter, Re) which varies from 4500 to 10,000. This range is equivalent to Reynolds number based on the spheres diameters, Re_d to change from 920 to 2570. An initial period of approximately 25–30 min was required before reaching the steady-state conditions (temperatures indicated by the thermocouples did not vary with more than ±0.1 °C within a period of about 10 min). At the end of each test and after collecting a set of data at steady-state condition, the volumetric flow rate of the injected air or the rate of supplied power was changed to collect a new set of data.

3. Analysis

3.1. Pressure drop

The pressure drop was measured by a U-type manometer and Eq. (1) is used to calculate the friction factor for different conditions of flow [46].
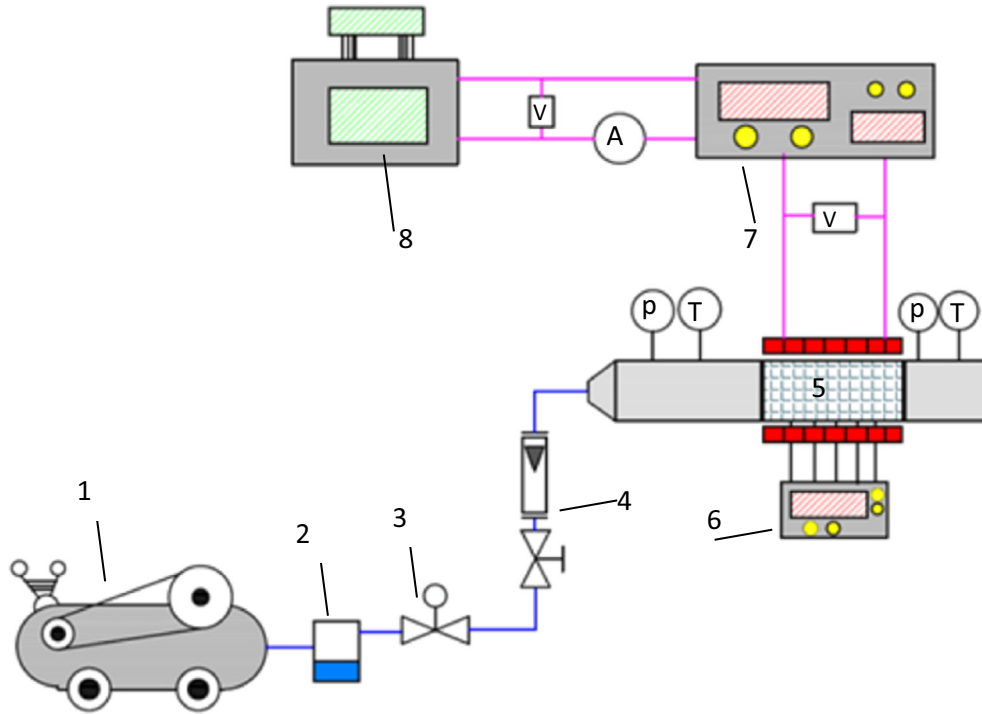
Fig. 1a. Schematic of the experimental set-up. 1: compressor, 2: water filter, 3: pressure regulator, 4: volumetric flow meter, 5: test section, 6: digital thermometer, 7: heating system controller, and 8: power supply.
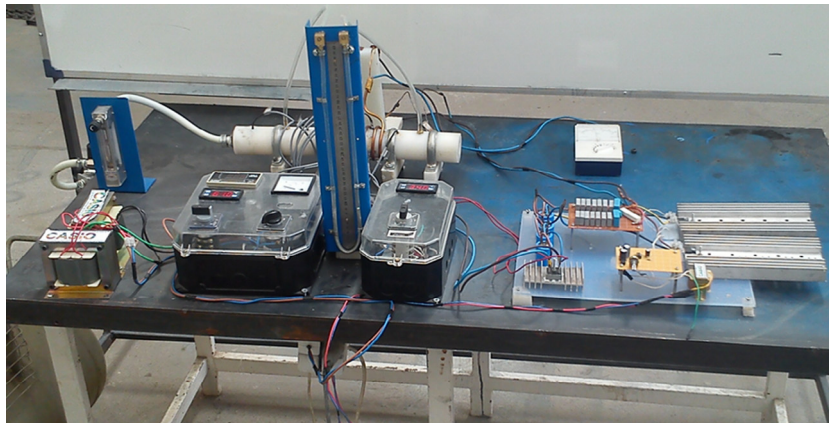
Fig. 1b. Experimental set-up.

$$f = \frac{2\Delta P}{\rho u^2} \frac{D}{L}, \tag{1}$$

where ΔP is the pressure drop along the channel length L and D is the channel diameter. u and ρ are respectively average velocity (measured in an empty channel) and density of air in the test section.

3.2. Heat transfer

The rate of generated heat inside the test section was calculated by Eq. (2) as follow:

$$Q = \dot{m}c_p(T_{out} - T_{in}), \tag{2}$$

where c_p is the air specific heat at constant pressure and $\dot{m}$ is the air mass flow rate. T_{in} and T_{out} are the inlet and outlet temperatures of air, respectively.

The average heat transfer coefficient is obtained by Newton's law of cooling [36,46]:

$$\bar{h} = \frac{Q}{A(\overline{T}_s - \overline{T}_f)}, \tag{3}$$

$$A = \pi d^2 N, \tag{4}$$

$$\overline{T}_s = \frac{1}{5}\sum_{i=1}^{5} T_{si}, \tag{5a}$$

$$\overline{T}_f = \frac{1}{5}\sum_{i=1}^{5} T_{fi}, \tag{5b}$$

where A is the heat transfer area, d is the spheres diameter, N is number of spheres, T_s and T_f are spheres and fluid (air) tempera-
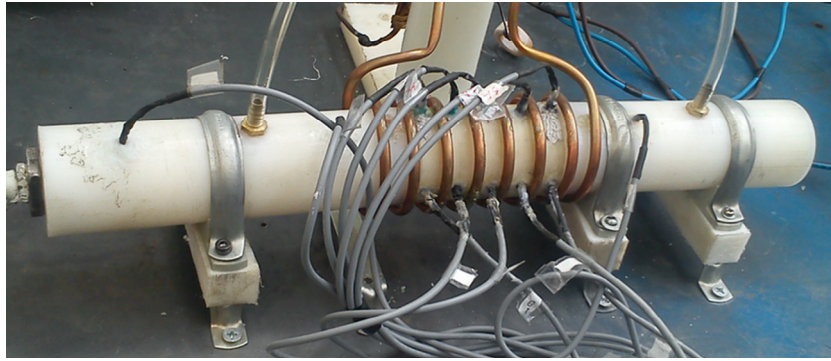
Fig. 2a. Test section.
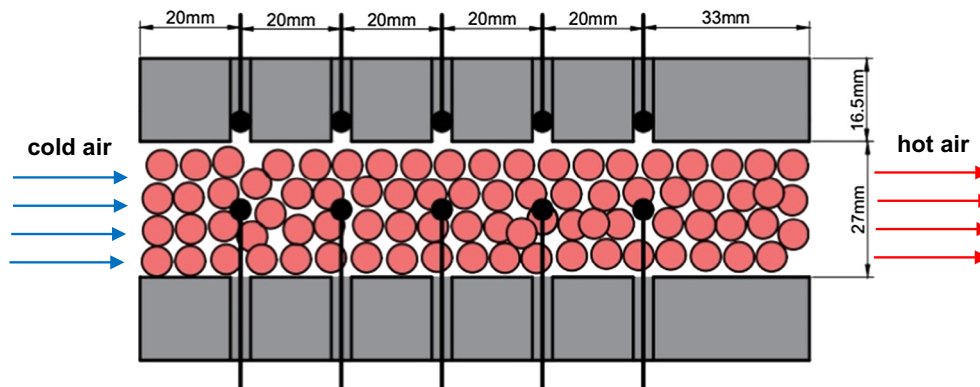
Fig. 2b. Schematic of the test section.

tures, respectively. The average Nusselt number is evaluated by [22,28,52–56]:

$$Nu = \frac{\bar{h}\, d}{k},\qquad(6)$$

where k is the thermal conductivity of the air and d is the sphere diameter.

Local heat transfer coefficient at a position of x along the test section can be obtained as [36]:

$$h_x = \frac{Q_x}{A_x(T_{sx} - T_{fx})},\qquad(7)$$

where T_{sx} and T_{fx} are local temperature for sphere and air phases, respectively within the pebble bed. $Q_x = Q(x/L)$ is the total generated heat for the spheres from the inlet of the channel to a position x. $A_x = A(x/L)$ is the total area of the spheres (see Eq. (4)) located in a distance from the channel inlet to a position x. As shown in Fig. 2b for the test section, the sensors were located in five locations along the axial direction of the channel, which divided the test section into four segments. In each location (x) there are two sensors, one was located near the channel wall at a distance about 1 mm from spheres to measure the air temperature. And another sensor was embedded between spheres inside the channel to measure the spheres surface temperature. The following assumptions were used to calculate the local heat transfer coefficients [36,57]. At each x-location the spheres temperature along the pipe radius are uniform and thus the sensor measurements at each x-position represents the average temperature of the spheres at this location [36,57]. It is also assumed that for each x-location the air temperature measured near the channel wall (that is near the sphere close to the wall) represents the average temperature of the air at x-location, and thus uniform air temperature is assumed at each x-location.

It should be pointed out that in this problem the objective is to remove heat from the heated spheres using air as the cooling fluid. Therefore, the heat transfer coefficient is defined as the ratio of total heat given to the spheres divided by the temperature differential between the fluid air and solid sphere, with A as the contact surface area between air and spheres.

3.3. Second law analysis

The pebble bed nuclear reactor that generates heat in a power plant involves the exergy content [58]. It is well known that heat transfer and pressure loss occur simultaneously in a porous channel [32,46]. Therefore, it is important to find a favorable working range at which heat transfer and pressure loss are in a tradeoff. Second law analysis of thermodynamics is a good method to optimize a system that exchanges heat between solid and fluid phases and also increases the pressure drop inevitably. Both temperature difference and friction are the main sources of entropy generation and consequently exergy destruction in a heat generating system that is cooled by a gas. Second law analysis has not been yet done in the pebble bed channel with internal heat generation. Because of the absence of second law analysis in the porous channel with internal heat generation, present study tries to reveal some aspect of second law analysis in a pebble bed cylindrical channel with internal heat generation. Thus, in order to obtain the favorable working rang of independent variables (such as generated heat, volumetric flow rate and spheres diameter), we consider relevant parameters including exergy transfer Nusselt number, entropy generation number and merit function. These parameters were presented by Wu et al. [59] and Zimparov [60] for double pipe heat exchanger and ducts with constant wall heat flux. They further used by Kurtbas et al. [46] for transport in rectangular channel

filled with foam with constant wall heat flux. But, in the present study these parameters are extended to analysis second law of thermodynamic in a pebble bed cylindrical channel with internal heat generation. Here we only present the extended relations for these parameters, and the details of driving the associate relations are described in Appendix A. The mean exergy transfer Nusselt number is written as:

$$\text{Nu}_e = \text{Nu}\left[1 - \frac{\pi \text{RePr}}{4N_Q N_T}\left(1 + \frac{f\pi \text{Re}^3}{8N_{QV}}\right)\ln\left(1 + \frac{4N_Q}{\pi \text{RePr}}\right)\right]. \tag{8}$$

Entropy generation considers losses because of finite temperature difference, fluid resistance and environment (which is usually ignored) [46,60]. Total irreversibility are presented as follows:

$$\dot{S}_{gen} = \frac{4\dot{m}c_p \Delta T_{sf}^2 d^2 N\text{St}}{D^2 T_{in}^2}\left(\frac{1}{1 + \frac{4d^2 N\Delta T_{sf}\text{St}}{D^2 T_{in}}}\right) + \frac{\dot{m}fu^2 LD}{8d^2 N\Delta T_{sf}\text{St}}$$
$$\times \ln\left(1 + \frac{4d^2 N\Delta T_{sf}\text{St}}{D^2 T_{in}}\right), \tag{9}$$

where $\dot{S}_{gen}$ is total irreversibility because of heat transfer and fluid friction. The first and second terms in the right-hand side of Eq. (9) express the entropy generation owing to heat transfer because of finite temperature difference and owing to flow resistance, respectively. Eqs. (8) and (9) are only valid for the cylindrical channel flow with uniform internal heat generation and thermally and hydrodynamically fully developed flow. In this work using entropy generation number (N_s) the irreversibility in the system is explained [46,60] as follow:

$$N_s = \frac{\dot{S}_{gen}}{\dot{m}c_p}. \tag{10}$$

For exergy analysis performed in this work we considered few parameters including entropy generation number (N_s), merit function (MF), mean exergy transfer Nusselt number (Nu_e), lost exergy transfer Nusselt number due to pressure drop (Nu_{eP}), and exergy transfer Nusselt number due to temperature difference (Nu_{eT}). Nu_e, Nu_{eT} and Nu_{eP} can be obtained using Eq. (8) as follow. According to Eq. (8) the mean exergy transfer Nusselt number is equal to the difference between the average Nusselt number and irreversibility of the heat transfer process in the porous channel with internal heat generation. Thus, Eq. (8) is re-written as:

$$\text{Nu}_e = \text{Nu}_{eT} - \text{Nu}_{eP}, \tag{11}$$

where Nu_{eT} is the exergy transfer Nusselt number caused by temperature difference and is equal to:

$$\text{Nu}_{eT} = \text{Nu}\left[1 - \frac{\pi \text{RePr}}{4N_Q N_T}\ln\left(1 + \frac{4N_Q}{\pi \text{RePr}}\right)\right]. \tag{12}$$

Nu_{eP} in Eq. (11) is the lost exergy transfer Nusselt number caused by the flow resistance and is written as:

$$\text{Nu}_{eP} = \frac{\pi^2 f \text{Re}^4 \text{PrNu}}{32 N_Q N_T N_{QV}}\ln\left(1 + \frac{4N_Q}{\pi \text{RePr}}\right). \tag{13}$$

The other parameter used to analyze the exergy transfer is merit function, which is given by Eq. (14). The MF expresses the ratio of exergy transfer to the sum of exergy transfer and exergy destruction [46]:

$$\text{MF} = \frac{E_q}{E_q + \dot{I}}, \tag{14}$$

where E_q is the exergy transfer due to energy transfer at the rate of Q:

$$E_q = Q\left(1 - \frac{T_0}{T_s}\right). \tag{15}$$

Higher values of the merit function indicates that the rate of increase in exergy transfer due to heat transfer dominates the rate of increase of the irreversibility [46], and thus higher values of the merit function are preferred [46].

4. Results and discussion

4.1. Validation

In order to confirm the accuracy and validation of the present experimental results, the pressure drop and mean Nusselt number are studied here. These parameters are obtained in the present work under steady state condition for the fully developed region of the channel, and are compared against previous experimental data and available correlations. The relevant correlations for the pressure drop are developed by Ergun [61], Vafai et al. [62] and Lee and Ogawa [63] as follows.

Ergun [61]

$$\frac{\Delta P}{L} = 150\frac{(1-\varepsilon)^2 \mu u}{\varepsilon^3 d^2} + 1.75\frac{(1-\varepsilon)\rho u^2}{\varepsilon^3 d}. \tag{16}$$

Vafai et al. [62]

$$\frac{\Delta P}{L} = 120\frac{(1-\varepsilon)^2 \mu u_D}{\varepsilon^3 d^2} + 2.3\frac{(1-\varepsilon)\rho u_D^2}{\varepsilon^3 d}, \tag{17}$$

where ε, u and $u_D = \varepsilon u$ in the above equations are porosity, average velocity and Darcy velocity, respectively.

Lee and Ogawa [63]

$$\frac{\Delta P}{L} = 12.5\frac{(1-\varepsilon)^2 \rho u^2}{2\varepsilon^3 d}(29.32\text{Re}_d^{-1} + 1.56\text{Re}_d^{-n} + 0.1), \tag{18}$$

where $\text{Re}_d = \frac{\rho u d}{\mu}$ is Reynolds number based on spheres diameter and $n = 0.352 + 0.1\varepsilon + 0.275\varepsilon^2$.

The pressure drop of the flowing air inside the porous channel, which filled with steel sphere with d = 7.5 mm versus Reynolds number, Re_d (based on the spheres diameter) is shown in Fig. 3a. In general, the measured pressure drops are in good agreements with those calculated by Eqs. (17) and (18). As discussed in Ref. [63] few parameters such as particles shape, surface roughness and particle distribution of the packed bed affect the friction factor and pressure drop in the pebble bed channel [63]. For Re_d > 1000, Ergun equation [61] is not exact enough and predicts much higher values than experimental data [63].

To further validate the present experimental data, we compare the average Nu number in the fully developed region of the present test section with previous experimental data as well as the correlations presented by Nie et al. [51], Wakao and Kaguei [55], Kuwahara et al. [56], Whitaker [64], Kays and London [65], Nsofor and Adebiyi [66], Incropera and DeWitt [67] and Bird et al. [68].

- Nie et al. [51] proposed the following correlation for the convective heat transfer coefficient in a spherical packed bed based on an experimental investigation for steady state condition.

$$\text{Nu} = \frac{hd}{k} = 0.052\frac{(1-\varepsilon)^{0.14}}{\varepsilon}\text{Re}_d^{0.86}\text{Pr}^{1/3}. \tag{19}$$

- Wakao and Kaguei [55] conducted experimental investigations and assembled both steady and unsteady data together. They proposed the following correlation for the interfacial convective heat transfer coefficient, which is valid only for packed bed with $\varepsilon \approx 0.4$.
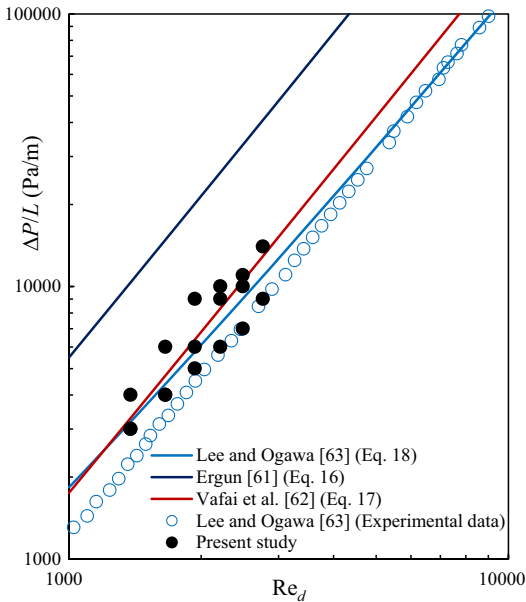
Fig. 3a. Pressure drop in the cylindrical channel versus Re_d number for sphere diameter of $d = 7.5$ mm compared with predicted data using Ergun equation [61], Vafai et al. [62] and Lee and Ogawa [63].

$$Nu = \frac{hd}{k} = 2 + 1.1Re_d^{0.6}Pr^{1/3}. \tag{20}$$

- Kuwahara et al. [56] developed the following correlation from numerical experiments based on the two-dimensional model for square shape particles in a packed bed.

$$Nu = \frac{hd}{k} = \left(1 + \frac{4(1-\varepsilon)}{\varepsilon}\right) + \frac{1}{2}(1-\varepsilon)^{1/2}Re_d^{0.6}Pr^{1/3}. \tag{21}$$

- Whitaker [64] using experimental data recommended the following correlation for forced convection heat transfer coefficient in a packed bed.

$$Nu = \frac{hd}{k} = \left[0.5Re_d^{-0.1}\left(\frac{(1-\varepsilon)^{0.5}}{\varepsilon}\right) + 0.2Re_d^{1/15}\left(\frac{(1-\varepsilon)^{1/3}}{\varepsilon}\right)\right]Re_d^{0.6}Pr^{1/3}. \tag{22}$$

- Kays and London [65] introduced the following correlation for heat transfer coefficient in a packed bed.

$$Nu = \frac{hd}{k} = 0.26\frac{(1-\varepsilon)^{0.3}}{\varepsilon}Re_d^{0.7}Pr^{1/3}. \tag{23}$$

- Nsofor and Adebiyi [66] based on an experimental investigation correlate the following relation for heat transfer coefficient in a packed bed made of cylindrical particles.

$$Nu = \frac{hd}{k} = 8.74 + 9.34Re_d^{0.2}Pr^{1/3}. \tag{24}$$

- Incropera and DeWitt [67] presented the following relation for heat transfer coefficient in non-spherical packed bed.

$$Nu = \frac{hd}{k} = \frac{0.79}{\varepsilon}Re_d^{0.425}Pr^{1/3}. \tag{25}$$

- Bird et al. [68] suggested the following correlation to use for heat transfer coefficient in non-spherical packed bed.

$$Nu = \frac{hd}{k} = 0.534Re_d^{0.59}Pr^{1/3}. \tag{26}$$

Fig. 3b shows the average Nusselt number for the steady state condition obtained in the present experiment (with $d = 5.5$ mm and $\varepsilon = 0.45$), compared with the previous experimental data of

Wakao and Kaguei [55] and the correlations given in Eqs. (19)–(26). It is seen that the Nusselt number obtained based on the present experiment are in a good agreement with the results obtained using the correlation developed by Nie et al. [51] (Eq. (19)). But, the present results show discrepancy with other correlations. Correlations presented by Eqs. (21), (25) and (26) are valid for non-spherical packed bed. In addition, Eqs. (20), (22) and (23) are valid for spherical but not purely steady state flow regime. While, the results predicted by Nie et al. [51] and those obtained in the present work are obtained for spherical particles under steady state condition.

Kuwahara et al. [56] commented that the correlation proposed by Wakao and Kaguei [55], which was obtained by combining steady and unsteady data, need to be corrected. Because their [56] unsteady numerical solutions suggested that a separate equation should be established for correlating the unsteady data. Also in Ref. [51] discussed that Nsofor and Adebiyi [66] experimentally investigated cylindrical particles at very high temperature to correlate Eq. (24). In such high temperature, radiation and free convection heat transfer must be contributed to develop a correlation. While these important effects were not included in the correlation developed by Nsofor and Adebiyi [66] given by Eq. (24).

It is further discussed by Nie et al. [51] that in the works by Whitaker [64] and, Kays and London [65], the thermocouples used to measure the particles surface temperature were not glued to the particles. Therefore, the temperature of the solid surface may be affected by the fluid temperature in Refs. [64,65] and thus may not be accurately measured.

4.2. Pressure drop and friction factor

The effect of sphere diameter on the pressure drop is shown in Fig. 4. For a fixed Re_d number, by decreasing the diameter of the steel balls, the pore size decreases. Consequently the net cross sectional area of the flow decreases. This results to an increase in the resistance to the fluid flow and thus, the pressure drop along the channel increases.

As shown in Fig. 5 the friction factor (f) inside the porous channel is a function of Re_d number and also the diameter of the steel balls. For a fixed Re_d number, decreasing the diameter of steel balls increases the resistance to the air flow and thus the friction factor
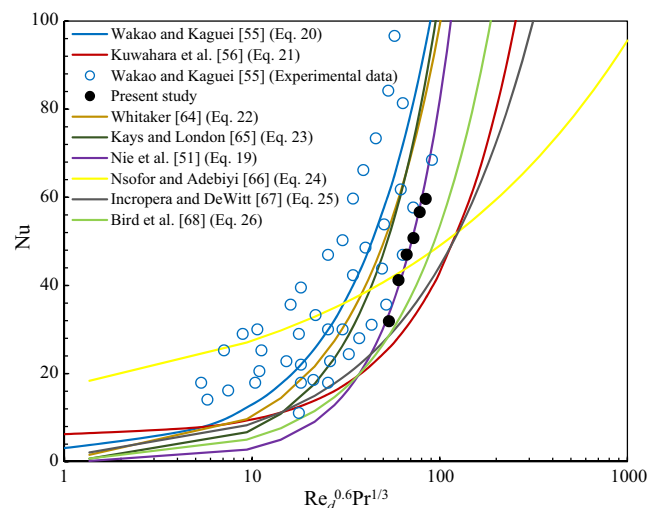
Fig. 3b. Average Nusselt number in the fully developed region obtained using the present experimental data for heat generation of $Q = 71.52$ W and sphere diameter of $d = 5.5$ mm compared with the previous experimental work [55], and previous correlations given in Refs. [51,55–56,64–68].

and pressure drop increase. Furthermore, as we expect for a fixed sphere diameter, as Re_d number increases the friction factor decreases.

4.3. Nusselt number

The variation of local Nusselt number (Nu_x) for the pebble bed channel filled by steel balls with d = 5.5 mm is shown in Fig. 6. The rate of generated heat inside the porous media is Q = 71.52 W, which transfers to the air flow by forced convection mechanism. Fig. 6 shows that for a fixed air volumetric flow rate although Nu_x decreases along the channel, from x = 8 cm to the end of the cylindrical channel, Nu_x is almost constant in the fully developed region of the channel. It is also seen that for a fixed position along the channel, by increasing the volumetric flow rate, the local Nusselt number increases. Because, for a constant cross section of the channel, by increasing the volumetric flow rate, the air velocity increases. The higher velocity of the flow causes the fluid that has already exchanged heat with the spheres, to be replaced with the fresh cold air. This results in lower temperature difference between the fluid air and solid spheres. Thus, according to Eq. (7) the local heat transfer coefficient and consequently Nu number increases.

Fig. 7a displays the variation of the average Nu number with Re_d number at different rates of internal generated heat for spheres with d = 5.5 mm. It is seen that Nu increases with the increase of Re_d number. Because for a higher flow rate (which is equivalent to higher air velocity and Re_d number), the internal convection heat exchange between the fluid and solid particles increases. This results in a lower temperature difference between the two phases (see Fig. 7b) and thus higher Nu number. Therefore, according to Eq. (7) the local heat transfer coefficient increases and consequently the Nu number increases, as shown in Fig. 7a.

Fig. 7a also shows that for a fixed Re_d number, increasing the rate of generated heat inside the channel does not have significant influence on the Nu number. Here we see that for a fixed Re_d number, increasing Q by 50% increases Nu number within 10%. This indicates that changes in the internal heat generation do not significantly affect the rate of heat transfer from solid sphere to the cooling air. This observation is in agreement with those of Meng et al. [36]. In their experiment [36] with water as the working fluid, it was observed that for a fixed Re number when increasing the internal heating power from 10 to 50 kW, the heat transfer coefficient of the channels is within 5%.

Fig. 5. Friction factor versus Re_d number for different spheres diameters.

Fig. 6. Local Nusselt number along the channel length for spheres with d = 5.5 mm and heat generation of Q = 71.52 W at different volumetric flow rates, $\dot{V}$.

Fig. 7a. Nusselt number versus Re_d number for sphere diameter of d = 5.5 mm and different heat generations, Q.

Fig. 4. Pressure drop in the packed bed channel versus Re_d number for different spheres diameters. (For the graphs provided in the paper, lines are not curve-fits. They are used only to connect the experimental data points for better observation of the variations.)
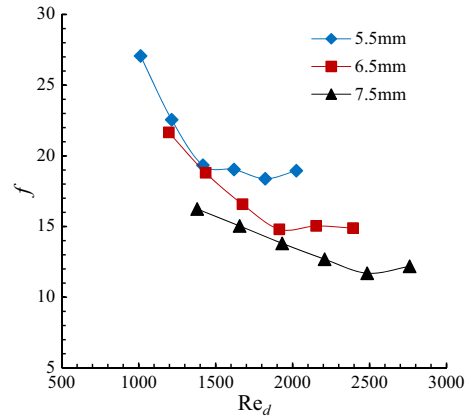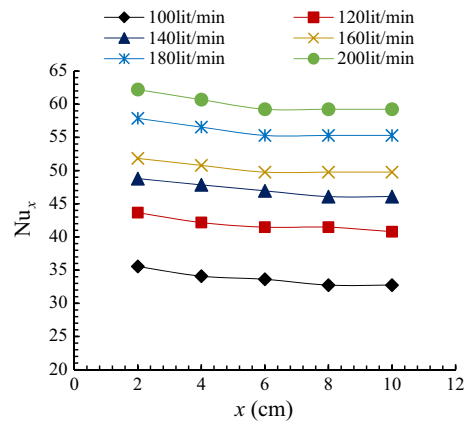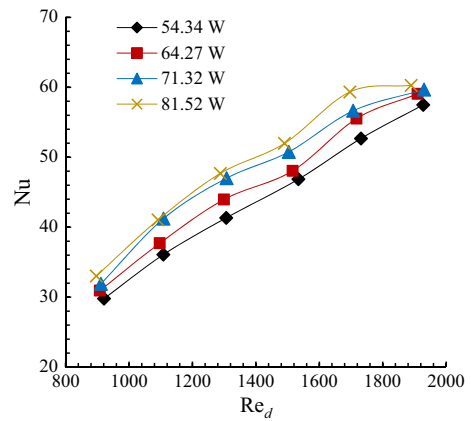
The influence of the diameter of steel balls on Nu number is illustrated in Fig. 8 as a function of Re_d number. It can be seen that for a fixed Re_d number, Nu increases with decreasing d. Because according to Eq. (4) the contact total surface area A between the particles and the air flow increases with decreasing particle diameter, which intensifies the convection heat transfer. Thus, the pebble bed with smaller diameter particles has a better heat transfer intensity. This observation is in accord with the previous
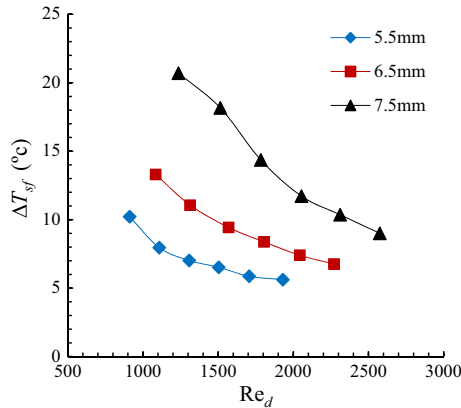
Fig. 7b. Mean temperature difference between the fluid and solid phases versus Re_d number for different spheres diameters and generated heat of $Q = 71.52$ W.
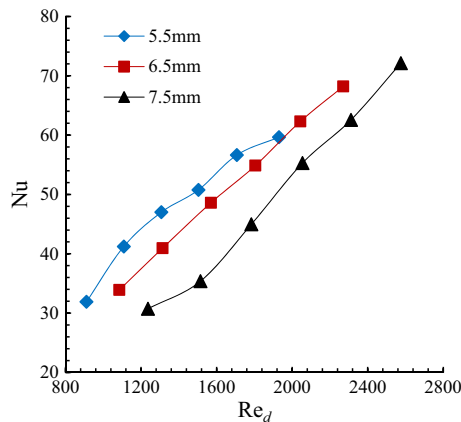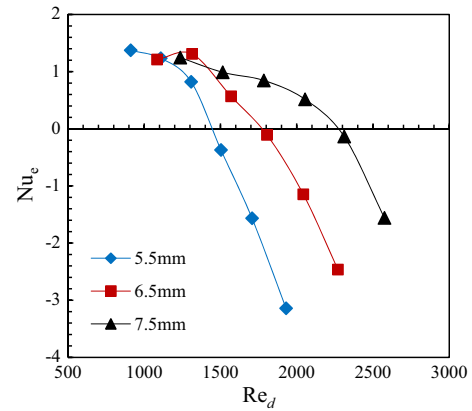

Fig. 9. Mean exergy transfer Nusselt number, Nu_e versus Re_d number for different spheres diameters with heat generation of $Q = 71.52$ W.

Fig. 8. Nusselt number versus Re_d number for heat generation of $Q = 71.52$ W and different spheres diameters.
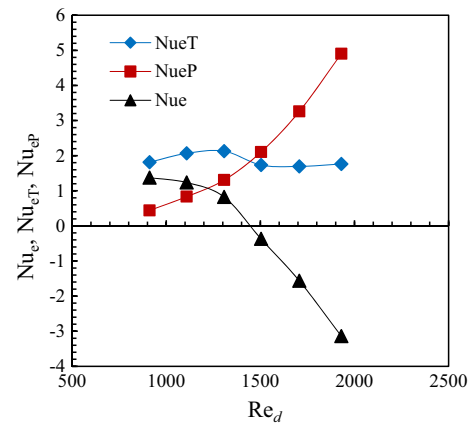

Fig. 10. Mean exergy transfer Nusselt number (Nu_e), exergy transfer Nusselt number caused by temperature difference (Nu_{eT}), and lost exergy transfer Nusselt number (Nu_{eP}) versus Re_d number for sphere diameter of $d = 5.5$ mm and heat generation of $Q = 71.52$ W.

experimental results of Meng et al. [36]. Also decreasing the spheres diameter makes the cavities between the spheres become smaller. Therefore, for a constant flow rate, the local velocity in the cavities increases. This increases the rate of heat transfer from heated spheres to the flowing air, and thus the Nu number increases [46].

4.4. Exergy transfer and irreversibility

In this section, exergy transfer and irreversibility characteristics of cylindrical porous channel flow with uniform internal heat generation are discussed. Results presented in this section consist of entropy generation number (N_s), merit function (MF), mean exergy transfer Nusselt number (Nu_e), lost exergy transfer Nusselt number due to friction (Nu_{eP}), and exergy transfer Nusselt number due to temperature difference (Nu_{eT}).

Fig. 9 demonstrates the variation of Nu_e as a function of Re_d number for different spheres diameter and heat generation of $Q = 71.52$ W. As seen in Fig. 9, for a fixed heat generation Q and sphere diameter d, with the increase of Re_d, the mean exergy transfer Nusselt number Nu_e, decreases until it become zero for a critical Re_d number. According to Eq. (11) Nu_e becomes zero, when $Nu_{eT} = Nu_{eP}$. This will be discussed later. The critical Re_d number are about 1450, 1800 and 2300 for $d = 5.5$, 6.5 and 7.5 mm, respectively. Further increase in Re_d number above the critical value, decreases Nu_e to negative values. Negative Nu_e indicates that the

irreversibility ratio of the system increases [46], because exergy transfer due to heat transfer is less than the exergy loss due to the flow friction.

Fig. 10 shows that the exergy transfer Nusselt number due to temperature difference (Nu_{eT}) remains almost constant as the Re_d number increases. While the exergy loss Nu number (Nu_{eP}) increases sharply with the increase of Re_d number. The zero values of Nu_e observed in Fig. 9, are associated with Re_d numbers when $Nu_{eT} = Nu_{eP}$. This equality indicates that exergy transfer due to temperature difference is equal to loss of exergy transfer due to flow resistance. However, as Re_d number increases, Nu_{ep} increases, while Nu_{eT} remains almost constant (see Fig. 10). Thus, the total Nu_e becomes negative as can be seen in Figs. 9 and 10.

Fig. 11 shows the effect of the internal heat generation on Nu_e. Similar to the variation of Nu shown in Fig. 7a it is seen that the internal heat generation has a negligible effect on Nu_e.

The other parameter that describes the irreversibility in the heat transfer system is the entropy generation. Dimensionless form of irreversibility is non-dimensional exergy destruction (N_s), which is called entropy generation number. By minimizing N_s a thermodynamically optimum state can be obtained for heat transfer process [46]. Fig. 12 presents variation of N_s versus Re_d number for different spheres diameters for heat generation of $Q = 71.52$ W. It is seen that for $d = 5.5$ and as Re_d increase the non-dimensional exergy destruction number N_s, increases sharply. For higher d it
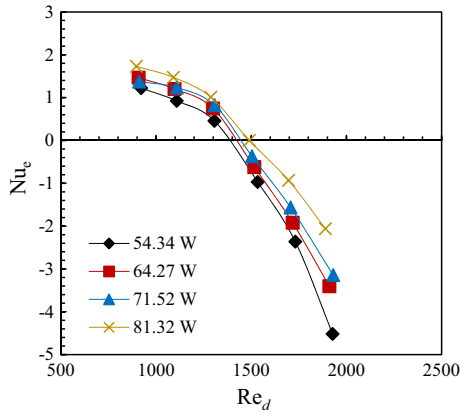
Fig. 11. Mean exergy transfer Nusselt number (Nu_e) versus Re_d number for spheres diameter of d = 5.5 mm at different heat generations.
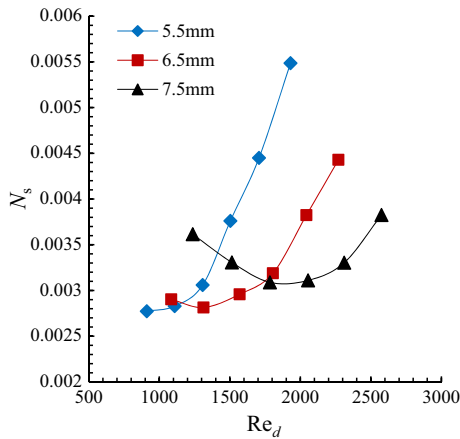

Fig. 12. Entropy generation number, N_s versus Re_d number for different spheres diameters with heat generation of Q = 71.52 W.
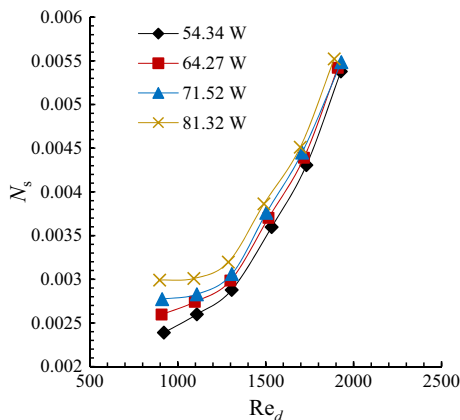

Fig. 13a. Entropy generation number, N_s versus Re_d number for spheres diameter of d = 5.5 mm at different heat generations.

is seen that N_s decreases with the increase of Re_d number up to a critical Re_d number. Further increase in the Re_d number, increases N_s. It is seen that for Re_d > 1800 and for a fixed Re_d number, as the sphere diameter decreases the value of entropy generation N_s, increases.

From Fig. 12 it is seen that for a fixed d_p, there is a critical Re_d number, which minimizes the entropy generation. For instance for d_p = 7.5 mm the entropy generation is minimum at Re_d = 2000. Furthermore, this figure also shows that for high Re_d > 1800, spheres with highest diameter (i.e. d_p = 7.5 mm) yield the minimum entropy generation number and thus maybe preferred to be used in the pebble bed channel for the purpose of cooling. One may also conclude that for low Re_d numbers, spheres with smaller diameter have low entropy generation number and preferred to use in the pebble bed.

Effect of variation of heat generation on the entropy generation number is presented in Fig. 13a. It is observed that for a fixed Re_d number, the entropy generation number, N_s increases with the increase of heat generation. Because as it shown in Fig. 13b for a fixed Re_d number, by increasing the generated heat, the temperature difference between solid and fluid phases increases. So irreversibility increases. This figure further shows that the effect of Q on N_s is more profound at low Re_d numbers. While for high particle Reynolds numbers, the effect in generated heat on the entropy generation is minor.

The last parameter that used to explain the performance of the heat transfer process is Merit function (MF) given by Eq. (14). Fig. 14 shows the variation of MF versus Re_d number for different spheres diameters. This figure shows that for a fixed sphere diameter, the merit function increases as Re_d number decreases. Increasing the merit function shows that exergy transfer due to heat transfer dominates the exergy destruction and irreversibility in the system [46].

The effect of generated heat on merit function is shown in Fig. 15. The figure shows that for a fixed Re_d number as Q increases, the merit function increases. This effect is more profound at high Re_d numbers. From Figs. 14 and 15, it can be concluded that spheres with high diameters, low Re_d numbers and high heat generation, result in high merit function, and thus maybe preferred for the purpose of cooling in a packed bed.

4.5. Experimental uncertainty analysis

Experimental uncertainty of the convective heat transfer process is mainly introduced by the experiments errors, error calculations and accuracy of the measurement equipment. In the current work, the maximum errors are associated with the temperature sensors, volumetric flow meter, and U-type manometer, are respectively ±0.1 °C, ±5 lit/min and ±0.5 mm. The uncertainty analysis is calculated using the method by Kline and McClintock [69]. The uncertainty equation are generally presented as:

$$U_R = \left[\sum_{i=1}^{n} \left(\frac{\partial R}{\partial V_i} U_{V_i} \right)^2 \right]^{\frac{1}{2}}, \tag{27}$$

where R and V_i, $1 \le i \le n$, are dependent and independent variables respectively. U_R and U_{V_i} are the uncertainties for the dependent and the independent variables respectively. The relations to calculate uncertainty of heat transfer coefficient and Nusselt number are given in Appendix B. The non-dimensional form of Eq. (27) is $((U_R/R) \times 100)$ is presented to be in percentage [69–71].

The detailed procedure for the calculation of uncertainty is provided in Appendix B. For most of the results presented in the paper under conditions of d = 5.5 mm, Q = 71.52 W and volumetric flow rate of $\dot{V}$ = 140 lit/min we calculate the uncertainty for different pertinent parameters as described here. The uncertainty for the heat transfer surface area A is found to be 2.8%. We further obtained the uncertainty for the calculation of generated heat to be 3.5%. Eventually the uncertainties for the heat transfer coefficient and Nusselt number are found to be 4.9% and 5%, respec-
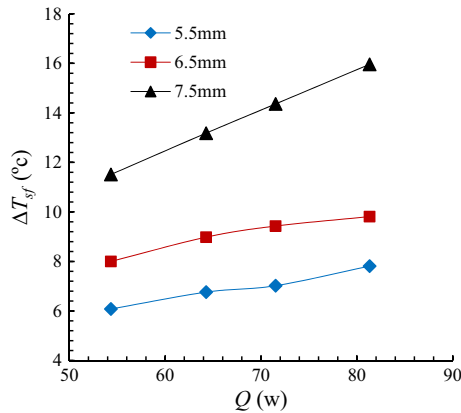
Fig. 13b. Mean temperature differences between fluid and solid phase for different spheres diameters and volumetric flow rate of $\dot{V}$ = 140 lit/min.
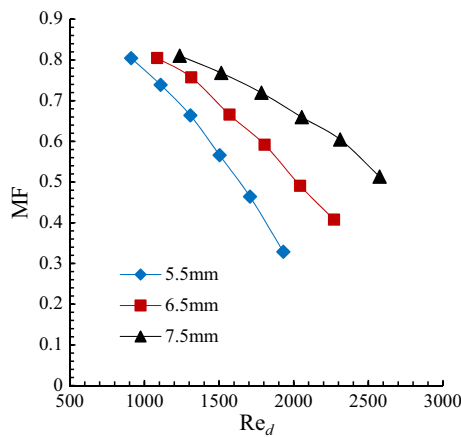

Fig. 14. Merit function, MF versus Re_d number for heat generation of Q = 71.52 W at different spheres diameters.
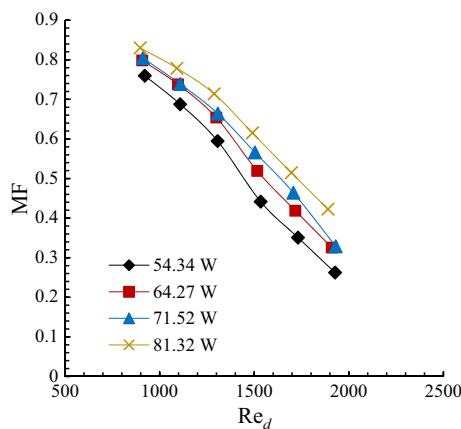

Fig. 15. Merit function MF, versus Re_d number for spheres diameter of d = 5.5 mm for different heat generations.

tively. The uncertainty obtained for the Nusselt number in the present work, is in a good agreement with those reported in other relevant experimental works (e.g. [46]), which reported the uncertainty of ~5.3%.

5. Conclusions

In this paper forced convection heat transfer in the cylindrical pebble bed channel with uniform internal heat generation in the turbulence flow regime was studied experimentally. Both analyses of the heat transfer and second law of thermodynamics were performed in order to find the optimum operating conditions forth purpose of cooling the packed bed channel. Internal heating was generated uniformly by electromagnetic induction heating method in metallic spheres. Compressed air was used as the working fluid in the experiments to extract heat from the heated spheres.

The major results of the present work can be summarized as follows:

- Nusselt number for air in the pebble bed channel increases with increasing the Reynolds number (Re_d) and decreasing the spheres diameter. Furthermore, an increase is observed in the pressure drop with increasing Re_d number and decreasing spheres diameter.
- For a fixed Re_d number, variation of internal heat generation found to have negligible effect on the Nusselt number, while the sphere diameter plays an important role on the variation of Nusselt number. For a fixed Re_d number increasing the sphere diameter decreases Nusselt number.
- For a fixed sphere diameter and internal heat generation, mean exergy transfer Nusselt number decreases with the increase of Re_d number, until it becomes zero for a critical Re_d number. The critical Re_d number are about 1450, 1800 and 2300 for d = 5.5, 6.5 and 7.5 mm, respectively. Further increase in Re_d number above the critical value, decreases Nu_e to negative values. Negative Nu_e indicates that the exergy transfer due to heat transfer is less than the exergy loss due to the flow friction.
- Similar to the Nu number, mean exergy transfer Nusselt number found to have negligible dependency on the internal heat generation, specifically at low Re_d numbers.
- For spheres with low diameter of 5.5 mm it is observed that as Re_d number increases the entropy generation number N_s, increases. While for higher spheres diameters and for a fixed heat generation Q, increasing Re_d number up to a critical Re_d number, decreases N_s. At the critical Re_d number, N_s yields the minimum value. For Re_d above the critical values, the entropy generation number increases with the increase of Re_d. The critical Re_d number are about 1800 and 2300 for spheres diameters of d = 6.5 mm and 7.5 mm, respectively.
- In addition, N_s analysis revealed that for values of Re_d higher than 1800, steel spheres with higher diameter yield lower N_s values.

Appendix A. Second law analysis

The exergy transfer equation of convective heat transfer is written based on the linear non-equilibrium thermodynamics theory as [46,59]:

$$E = h_{ex}\Delta T_{sf}A. \tag{A1}$$

Using the definition of specific flow exergy,

$$\acute{e} = f(T,P) = \acute{h} - \acute{h}_0 - T_0(s - s_0), \tag{A2}$$

the differential form of the specific flow exergy equation can be expressed as

$$d\acute{e} = \left(\frac{d\acute{e}}{dT}\right)_P dT_f + \left(\frac{d\acute{e}}{dP}\right)_T dP, \tag{A3}$$

$$\left(\frac{d\acute{e}}{dT}\right)_P = \left(\frac{d\acute{h}}{dT}\right)_P - T_0\left(\frac{ds}{dT}\right)_P, \tag{A4}$$

$$\left(\frac{d\acute{e}}{dP}\right)_T = \left(\frac{d\acute{h}}{dP}\right)_T - T_0\left(\frac{ds}{dP}\right)_T. \tag{A5}$$

By using the following thermodynamic relations:

$$\left(\frac{d\acute{h}}{dT}\right)_P = c_p, \tag{A6}$$

$$\left(\frac{ds}{dT}\right)_P = \frac{c_p}{T_f}, \tag{A7}$$

$$\left(\frac{ds}{dP}\right)_T = \frac{1}{T_f}\left(\frac{d\acute{h}}{dP}\right)_T - \frac{\vartheta}{T_f}, \tag{A8}$$

the deferential form of the specific flow exergy can be written as

$$d\acute{e} = c_p\left(1 - \frac{T_0}{T_f}\right)dT_f + \frac{T_0}{\rho T_f}dP. \tag{A9}$$

In the above equations T_0, is the ambient temperature, s is entropy, $\acute{h}$ is the specific enthalpy, $\acute{e}$ is specific exergy and ϑ is the specific volume.

The exergy transfer rate in a differential form along the channel length is given by

$$dE = h_{ex}\Delta T_{sf}dA = \dot{m}d\acute{e}, \tag{A10}$$

$$dE = h_{ex}\Delta T_{sf}dA = \dot{m}\left[c_p\left(1 - \frac{T_0}{T_f}\right)dT_f + \frac{\vartheta T_0}{T_f}dP\right], \tag{A11}$$

where

$$dA = \frac{\pi d^2 N}{L}dx \tag{A12}$$

and

$$\dot{m} = \rho u\frac{\pi D^2}{4}. \tag{A13}$$

Longitudinal temperature distribution of the fluid in the channel with internal heat generation can be written as

$$T_f = T_{in} + \frac{Q}{L\dot{m}C_p}x = T_{in} + \frac{Q}{L\rho u\frac{\pi D^2}{4}c_p}x = T_{in} + \frac{4Q\mathrm{St}}{\pi LD^2 h}x. \tag{A14}$$

By combining Eqs. (A14), (A13), (A12), (3) and (4) with Eq. (A11), the following relation is obtained:

$$h_{ex}\left(\frac{Q}{Lh}\right)dx = \frac{\rho u\pi D^2}{4}\left[c_p\left(1 - \frac{T_0}{T_{in} + \frac{4Q\mathrm{St}}{\pi LD^2 h}x}\right)dT_f + \frac{\vartheta T_0}{T_{in} + \frac{4Q\mathrm{St}}{\pi LD^2 h}x}dP\right]. \tag{A15}$$

From Eq. (A15) the local exergy transfer coefficient for cylindrical channel with internal heat generation is found as

$$h_{ex} = \frac{hL\rho u\pi D^2}{4Q}\left[c_p\left(1 - \frac{T_0}{T_{in} + \frac{4Q\mathrm{St}}{\pi LD^2 h}x}\right)\frac{dT_f}{dx} + \frac{\vartheta T_0}{T_{in} + \frac{4Q\mathrm{St}}{\pi LD^2 h}x}\frac{dP}{dx}\right], \tag{A16}$$

where St is Stanton number, (dT_f/dx) and (dP/dx) are temperature and pressure gradient along the cylindrical channel and can be written as [46,59]:

$$\mathrm{St} = \frac{h}{\rho u c_p}, \tag{A17}$$

$$\frac{dT_f}{dx} = \frac{4Q}{c_p L\rho u\pi D^2}, \tag{A18}$$

$$\frac{dP}{dx} = -\frac{f\rho u^2}{2D}. \tag{A19}$$

By combining Eqs. (A17), (A18), (A19) and (A16), the local exergy transfer coefficient can be written as:

$$h_{ex} = h\left[1 - \frac{T_0}{T_{in} + \frac{4Q\mathrm{St}}{\pi LD^2 h}x}\left(1 + \frac{f\pi\mathrm{Re}^3 L\mu^3}{8Q\rho^2 D^2}\right)\right]. \tag{A20}$$

One could introduce the non-dimensional relations as follows:

$$N_T = \frac{T_{in}}{T_0}, \tag{A21}$$

$$N_Q = \frac{Q}{T_{in}kD}, \tag{A22}$$

$$N_{QV} = \frac{Q\rho^2 D^2}{L\mu^3}. \tag{A23}$$

Then, by substituting Eqs. (A21)–(A23) into Eq. (A20), the local exergy transfer coefficient can be written as:

$$h_{ex} = h\left[1 - \frac{1}{N_T\left(1 + \frac{4N_Q}{\pi\mathrm{RePr}}\frac{x}{L}\right)}\left(1 + \frac{f\pi\mathrm{Re}^3}{8N_{QV}}\right)\right]. \tag{A24}$$

The relationship between the local and mean exergy transfer coefficient is as follow:

$$h_e = \frac{1}{L}\int_0^L h_{ex}dx. \tag{A25}$$

With the integration of Eq. (A24) along the channel length and in combination with Eq. (A25), the mean exergy transfer coefficient becomes:

$$h_e = h\left[1 - \frac{\pi\mathrm{RePr}}{4N_Q N_T}\left(1 + \frac{f\pi\mathrm{Re}^3}{8N_{QV}}\right)\ln\left(1 + \frac{4N_Q}{\pi\mathrm{RePr}}\right)\right]. \tag{A26}$$

Mean exergy transfer Nusselt number (Nu_e) is obtained as [46,59]:

$$\mathrm{Nu}_e = \frac{h_e d}{k}. \tag{A27}$$

From Eq. (A27) and Eq. (A26), the mean exergy transfer Nusselt number could be resulted from the following equation:

$$\mathrm{Nu}_e = \mathrm{Nu}\left[1 - \frac{\pi\mathrm{RePr}}{4N_Q N_T}\left(1 + \frac{f\pi\mathrm{Re}^3}{8N_{QV}}\right)\ln\left(1 + \frac{4N_Q}{\pi\mathrm{RePr}}\right)\right]. \tag{A28}$$

A heat transfer process inside thermal equipment involves some losses because of finite temperature difference, fluid resistance and environment (which is usually neglected) [46,60]. The increase of irreversibility of heat transfer process because of above mentioned losses can be calculated using Gouy-Stolda theorem as a function of entropy generation [46]:

$$I = T_0\dot{S}_{gen}, \tag{A29}$$

where $\dot{S}_{gen}$ is total irreversibility due to heat transfer and fluid friction. Zimparov [60] derived an equation for $\dot{S}_{gen}$ from the first and second law statements for a channel with constant wall heat flux.

In this work the Zimparov's method was extended to derive $\dot{S}_{gen}$ in the porous channel with internal heat generation. The rate of entropy generation is as follow [60]:

$$d\dot{s}_{gen} = \dot{m}ds - \frac{dQ}{T_f + \Delta T_{sf}}. \tag{A30}$$

Using thermodynamics relations $(T_f ds = dh - \vartheta dp)$, $(dh = c_p dT_f)$ and $(dQ = \dot{m}dh)$, Eq. (A30) can be written as

$$d\dot{s}_{gen} = \dot{m}c_p dT_f \left(\frac{1}{T_f} - \frac{1}{T_f + \Delta T_{sf}} \right) - \dot{m}\frac{\vartheta}{T_f} dP. \tag{A31}$$

Combining Eqs. (A18) and (A19) with Eq. (A31) the following relation is obtained:

$$\frac{d\dot{s}_{gen}}{dx} = \dot{m}c_p \left(\frac{4d^2 N St}{LD^2} \right) \frac{\Delta T_{sf}^2}{T_f^2 \left(1 + \frac{\Delta T_{sf}}{T_f} \right)} + \frac{\dot{m}}{T_f} \left(\frac{fu^2}{2D} \right). \tag{A32}$$

The first and the second terms in the right-hand side of Eq. (A32) express the entropy generation owing to heat transfer because of finite temperature difference and also due to flow resistance, respectively. By combining Eqs. (A32) and (A14), and knowing that when $\left(\frac{\Delta T_{sf}}{T_f} \ll 1 \right)$, $(\Delta T_{sf}/T_f)$ can be neglected, Eq. (A33) is obtained.

$$\frac{d\dot{s}_{gen}}{dx} = \dot{m}c_p \left(\frac{4d^2 N St}{LD^2} \right) \frac{\Delta T_{sf}^2}{T_{in}^2 \left[1 + \frac{4d^2 N\Delta T_{sf} St}{LD^2 T_{in}} x \right]^2} + \frac{\dot{m}fu^2}{\left[T_{in} \left(1 + \frac{4d^2 N\Delta T_{sf} St}{LD^2 T_{in}} x \right) \right] 2D}. \tag{A33}$$

By integrating Eq. (A33) along the length of the channel, the following relation for the entropy generation is demonstrated.

$$\dot{S}_{gen} = \frac{4\dot{m}c_p \Delta T_{sf}^2 d^2 N St}{D^2 T_{in}^2} \left(\frac{1}{1 + \frac{4d^2 N\Delta T_{sf} St}{D^2 T_{in}}} \right) + \frac{\dot{m}fu^2 LD}{8d^2 N\Delta T_{sf} St}$$

$$\times \ln \left(1 + \frac{4d^2 N\Delta T_{sf} St}{D^2 T_{in}} \right). \tag{A34}$$

Entropy generation number (N_s) is used to explain the irreversibility in the system [46,59] as follow:

$$N_s = \frac{\dot{S}_{gen}}{\dot{m}c_p}. \tag{A35}$$

Appendix B. Uncertainty

The independent measured variables considered to calculate the uncertainties of the experiment are reported in Table A1.

Based on Eqs. (2)–(4), (6) and (21), the relations to calculate the uncertainties in heat transfer coefficient and Nu number are presented as:

$$U_h = \left[\left(\frac{\partial h}{\partial Q} U_Q \right)^2 + \left(\frac{\partial h}{\partial A} U_A \right)^2 + \left(\frac{\partial h}{\partial T_s} U_{T_s} \right)^2 + \left(\frac{\partial h}{\partial T_f} U_{T_f} \right)^2 \right]^{1/2}, \tag{A36}$$

$$U_{Nu} = \left[\left(\frac{\partial Nu}{\partial h} U_h \right)^2 + \left(\frac{\partial Nu}{\partial d} U_d \right)^2 + \left(\frac{\partial Nu}{\partial k} U_k \right)^2 \right]^{1/2}, \tag{A37}$$

where U_{T_s} and U_{T_f} for solid and fluid phases are equal to U_T, which is given in the Table A1. U_Q and U_A are given as

$$U_Q = \left[\left(\frac{\partial Q}{\partial \dot{m}} U_{\dot{m}} \right)^2 + \left(\frac{\partial Q}{\partial C_p} U_{C_p} \right)^2 + \left(\frac{\partial Q}{\partial T_{out}} U_{T_{out}} \right)^2 + \left(\frac{\partial Q}{\partial T_{in}} U_{T_{in}} \right)^2 \right]^{1/2}, \tag{A38}$$

Table A1
Uncertainty of instruments.

Parameter	Nomenclature	Nomenclature of uncertainty
Temperature (°C)	T	U_T
Diameter of balls (m)	d	U_d
Mass flow rate (kg/s)	$\dot{m}$	$U_{\dot{m}}$
Number the spheres	N	U_N

Table A2
Specifications for the experimental results presented in the paper.

Measured variable	Nominal value	Accuracy
Temperature difference (°C), $\Delta T_{oi} = T_{out} - T_{in}$	26.3	±0.1
Temperature difference (°C), $\Delta T_{sf} = T_s - T_f$	7	±0.1
Diameter of the spheres (m), d	0.0055	±0.00005
Mass flow rate (kg/s), $\dot{m} = \rho \dot{V}$	0.0027	±9.5×10^{-5}
Number of spheres, N	473	±10

$$U_A = \left[\left(\frac{\partial A}{\partial d} U_d \right)^2 + \left(\frac{\partial A}{\partial N} U_N \right)^2 \right]^{1/2}, \tag{A39}$$

where $U_{T_{in}}$ and $U_{T_{out}}$ are equal to U_T which is given in Table A1. U_{C_p} and U_k are uncertainty for the specific heat at constant pressure and thermal conductivity, which are assumed to be zero.

The specifications of the experiment is presented in Table A2.

Here, the uncertainty analyses for the cited experiment presented in the paper ($d = 5.5$ mm, $Q = 71.52$ W, $\dot{V} = 140$ lit/min) is derived. For the heat transfer total surface area we have

$$U_A = \left[(2\pi dN U_d)^2 + (\pi d^2 U_N)^2 \right]^{1/2}, \tag{A40}$$

$$\frac{U_A}{A} = \left[\left(2\frac{U_d}{d} \right)^2 + \left(\frac{U_N}{N} \right)^2 \right]^{1/2}. \tag{A41}$$

By substituting the nominal and uncertainty values from Table A2 in Eq. (A41), the uncertainty for the heat transfer surface area A, is obtained to be 2.8%.

For the generated heat we use the following equation:

$$U_Q = \left[(c_p \Delta T_{oi} U_{\dot{m}})^2 + 2(\dot{m}c_p U_T)^2 \right]^{1/2}, \tag{A42}$$

$$\frac{U_Q}{Q} = \left[\left(\frac{U_{\dot{m}}}{\dot{m}} \right)^2 + 2 \left(\frac{U_T}{\Delta T_{oi}} \right)^2 \right]^{1/2}. \tag{A43}$$

Substituting the nominal and uncertainty values from Table A2 into Eq. (A43), the uncertainty for the generated heat is found to be 3.5%.

The uncertainty for the heat transfer coefficient is obtained using the following equation

$$U_h = \left[\left(\frac{Q}{A^2 \Delta T_{sf}} U_A \right)^2 + \left(\frac{1}{A\Delta T_{sf}} U_Q \right)^2 + 2 \left(\frac{Q}{A\Delta T_{sf}^2} U_T \right)^2 \right]^{1/2}, \tag{A44}$$

$$\frac{U_h}{h} = \left[\left(\frac{U_A}{A} \right)^2 + \left(\frac{U_Q}{Q} \right)^2 + 2 \left(\frac{U_T}{\Delta T_{sf}} \right)^2 \right]^{1/2}. \tag{A45}$$

Using data given in Table A2 the uncertainty for the heat transfer coefficient is gained to be 4.9%.

Finally we calculate the uncertainty for the Nusselt number using the following equation:

$$U_{Nu} = \left[\left(\frac{d}{k} U_h \right)^2 + \left(\frac{h}{k} U_d \right)^2 \right]^{1/2}, \tag{A46}$$

$$\frac{U_{\mathrm{Nu}}}{\mathrm{Nu}} = \left[\left(\frac{U_h}{h}\right)^2 + \left(\frac{U_d}{d}\right)^2 \right]^{1/2}. \tag{A47}$$

By substituting from Table A2 in Eq. (A47), the uncertainty for Nu number is obtained to be 5%.

References

[1] World Nuclear Performance, Report 2016, World Nuclear Association, Report No. 2016/001, June 2016.

[2] A.C. Kadak, A future for nuclear energy: pebble bed reactors, Int. J. Crit. Infrastruct. 1 (4) (2005) 330–345.

[3] C.H. Rycroft, G.S. Grest, J.W. Landry, M.Z. Bazant, Analysis of granular flow in a pebble-bed nuclear reactor, Phys. Rev. E 74 (2) (2006) 1–16, 021306.

[4] R. Abdulmohsin, Gas dynamics and heat transfer in a packed pebble-bed reactor for the 4th generation nuclear energy PhD Thesis, Missouri University of Science and Technology, 2013.

[5] C.G. Du Toit, The numerical determination of the variation in the porosity of the pebble bed core, in: Proceedings of 1st International Topical Meeting on High Temperature Reactor Technology (HTR2002), Petten, Netherlands.

[6] G.J. Auwerda, Core physics of pebble bed high temperature nuclear reactors PhD Thesis, Delft University of Technology, 2014.

[7] G. Lomonaco, W. Grassi, N. Cerullo, The influence of the packing on the fuel temperature hot spots in a particle-bed GCFR, Sci. Technol. Nucl. Installations (2009) Article ID: 291453.

[8] K. Vafai, Handbook of Porous Media, second ed., Taylor and Francis, Boca Raton, 2005.

[9] A. Chumpia, K. Hooman, Performance evaluation of single tubular aluminium foam heat exchangers, Appl. Therm. Eng. 66 (1) (2014) 266–273.

[10] A. Chumpia, K. Hooman, Performance evaluation of tubular aluminum foam heat exchangers in single row arrays, Appl. Therm. Eng. 83 (2015) 121–130.

[11] M. Odabaee, K. Hooman, Metal foam heat exchangers for heat transfer augmentation from a tube bank, Appl. Therm. Eng. 36 (2012) 456–463.

[12] K. Yang, K. Vafai, Analysis of temperature gradient bifurcation in porous media – an exact solution, Int. J. Heat Mass Transf. 53 (19) (2013) 4316–4325.

[13] K. Hooman, Heat transfer and entropy generation for forced convection through a microduct of rectangular cross-section: effects of velocity slip, temperature jump, and duct geometry, Int. Commun. Heat Mass Transfer 35 (9) (2008) 1065–1068.

[14] X.L. Ouyang, K. Vafai, P.X. Jiang, Analysis of thermally developing flow in porous media under local thermal non-equilibrium conditions, Int. J. Heat Mass Transf. 67 (2013) 768–775.

[15] Y. Mahmoudi, Constant wall heat flux boundary condition in micro-channels filled with a porous medium with internal heat generation under local thermal non-equilibrium condition, Int. J. Heat Mass Transf. 85 (2015) 524–542.

[16] Y. Mahmoudi, M. Maerefat, Analytical investigation of heat transfer enhancement in a channel partially filled with a porous material under local thermal non-equilibrium condition, Int. J. Therm. Sci. 50 (12) (2011) 2386–2401.

[17] Y. Mahmoudi, N. Karimi, K. Mazaheri, Analytical investigation of heat transfer enhancement in a channel partially filled with a porous material under local thermal non-equilibrium condition: effects of different thermal boundary conditions at the porous-fluid interface, Int. J. Heat Mass Transf. 70 (2014) 875–891.

[18] M. Dehghan, M.S. Valipour, S. Saedodin, Y. Mahmoudi, Thermally developing flow inside a porous-filled channel in the presence of internal heat generation under local thermal non-equilibrium condition: a perturbation analysis, Appl. Therm. Eng. 98 (2016) 827–834.

[19] Y. Mahmoudi, N. Karimi, Numerical investigation of heat transfer enhancement in a pipe partially filled with a porous material under local thermal non-equilibrium condition, Int. J. Heat Mass Transf. 68 (2014) 161–173.

[20] P.X. Jiang, X.C. Lu, Numerical simulation of fluid flow and convection heat transfer in sintered porous plate channels, Int. J. Heat Mass Transf. 49 (9) (2006) 1685–1695.

[21] B. Alazmi, K. Vafai, Constant wall heat flux boundary conditions in porous media under local thermal non-equilibrium conditions, Int. J. Heat Mass Transf. 45 (15) (2002) 3071–3087.

[22] M. Sozen, K. Vafai, Analysis of the non-thermal equilibrium condensing flow of a gas through a packed bed, Int. J. Heat Mass Transf. 33 (6) (1990) 1247–1261.

[23] M. Sozen, K. Vafai, Analysis of oscillating compressible flow through a packed bed, Int. J. Heat Fluid Flow 12 (2) (1991) 130–136.

[24] M. Sozen, K. Vafai, L.A. Kennedy, Thermal charging and discharging of sensible and latent heat storage packed beds, AIAA J. Thermophys. Heat Transfer 5 (4) (1991) 623–625.

[25] M. Sozen, K. Vafai, Longitudinal heat dispersion in porous beds with real-gas flow, AIAA J. Thermophys. Heat Transfer 7 (1) (1993) 153–157.

[26] K. Vafai, C.P. Desai, S.C. Chen, An investigation of heat transfer process in a chemically reacting packed bed, Num. Heat Transfer Part A: Appl. 24 (2) (1993) 127–142.

[27] A.V. Kuznetsov, K. Vafai, Analytical comparison and criteria for heat and mass transfer models in metal hydride packed beds, Int. J. Heat Mass Transf. 38 (15) (1995) 2873–2884.

[28] A. Amiri, K. Vafai, Transient analysis of incompressible flow through a packed bed, Int. J. Heat Mass Transf. 41 (24) (1998) 4259–4279.

[29] G.M. Chrysler, R.E. Simons, An experimental investigation of the forced convection heat transfer characteristics of fluorocarbon liquid flowing through a packed-bed for immersion cooling of microelectronic heat sources, AIAA/ASME Thermophysics and Heat Transfer Conference, Cryogenic and Immersion Cooling of Optics and Electronic Equipment, ASME HTD 131 (1990) 21–27.

[30] M.R. Izadpanah, H. Müller-Steinhagen, M. Jamialahmadi, Experimental and theoretical studies of convection heat transfer in a cylindrical porous media, Int. J. Heat Fluid Flow 19 (6) (1998) 629–635.

[31] M. Jamialahmadi, H. Müller-Steinhagen, M.R. Izadpanah, Pressure drop, gas hold-up and heat transfer during single and two-phase flow through porous media, Int. J. Heat Fluid Flow 26 (1) (2005) 156–172.

[32] P.X. Jiang, G.S. Si, M. Li, Z.P. Ren, Experimental and numerical investigation of forced convection heat transfer of air in non-sintered porous media, Int. J. Heat Mass Transf. 28 (6) (2004) 545–555.

[33] P.X. Jiang, M. Li, T.J. Lu, L. Yu, Z.P. Ren, Experimental research on convection heat transfer in sintered porous plate channel, Exp. Thermal Fluid Sci. 47 (10) (2004) 2085–2096.

[34] O. Bautista, F. Mendez, Internal heat generation in a discrete heat source: conjugate heat transfer analysis, Appl. Therm. Eng. 26 (17) (2006) 2201–2208.

[35] K. Atkhen, G. Berthoud, SILFIDE experiment: coolability in a volumetrically heated debris bed, Nucl. Eng. Des. 236 (19) (2006) 2126–2134.

[36] X. Meng, Z. Sun, G. Xu, Single-phase convection heat transfer characteristics of pebble-bed channels with internal heat generation, Nucl. Eng. Des. 252 (2012) 121–127.

[37] A. Bejan, Entropy Generation Through Heat and Fluid Flow, first ed., John Wiley and Sons Inc., New York, 1982.

[38] K. Hooman, H. Gurgenci, A.A. Merrikh, Heat transfer and entropy generation optimization of forced convection in porous-saturated ducts of rectangular cross-section, Int. J. Heat Mass Transf. 50 (11) (2007) 2051–2059.

[39] A. Bejan, Entropy generation minimization: the new thermodynamics of finite-size devices and finite-time processes, J. Appl. Phys. 79 (3) (1996) 1191–1218.

[40] I. Kurtbas, A. Durmus, H. Eren, E. Turgut, Effect of propeller type swirl generators on the entropy generation and efficiency of heat exchangers, Int. J. Therm. Sci. 46 (3) (2007) 300–307.

[41] K. Hooman, A. Ejlali, Entropy generation for forced convection in a porous saturated circular tube with uniform wall temperature, Int. Commun. Heat Mass Transfer 34 (4) (2007) 408–419.

[42] K. Hooman, A. Haji-Sheikh, Analysis of heat transfer and entropy generation for a thermally developing Brinkman-Brinkman forced convection problem in a rectangular duct with isoflux walls, Int. J. Heat Mass Transf. 50 (21) (2007) 4180–4194.

[43] M. Torabi, K. Zhang, G. Yang, J. Wang, P. Wu, Heat transfer and entropy generation analyses in a channel partially filled with porous media using local thermal non-equilibrium model, Energy 82 (2015) 922–938.

[44] M. Bashi, S. Rashidi, J.A. Esfahani, Exergy analysis for a plate-fin triangular duct enhanced by a porous material, Appl. Therm. Eng. 110 (2017) 1448–1461.

[45] R. Prommas, P. Rattanadecho, D. Cholaseuk, Energy and exergy analyses in drying process of porous media using hot air, Int. Commun. Heat Mass Transfer 37 (4) (2010) 372–378.

[46] I. Kurtbas, N. Celik, I. Dincer, Exergy transfer in a porous rectangular channel, Energy 35 (1) (2010) 451–460.

[47] M.R.I. Ramadan, A.A. E1-Sebaii, S. Aboul-Enein, E. E1-Bialy, Thermal performance of a packed bed double-pass solar air heater, Energy 32 (8) (2007) 1524–1535.

[48] K. Yang, K. Vafai, Analysis of heat flux bifurcation inside porous media incorporating inertial and dispersion effects-an exact solution, Int. J. Heat Mass Transf. 54 (25) (2011) 5286–5297.

[49] K. Yang, K. Vafai, Transient aspects of heat flux bifurcation in porous media: an exact solution, ASME J. Heat Transfer 133 (5) (2011) 052602.

[50] K. Vafai, K. Yang, A note on local thermal non-equilibrium in porous media and heat flux bifurcation phenomenon in porous media, Transp. Porous Media 96 (2013) 169–172.

[51] X. Nie, R. Besant, R. Evitts, J. Bolster, A new technique to determine convection coefficients with flow through particle beds, Trans. ASME J. Heat Transfer 133 (4) (2011) 041601.

[52] W.M. Rohsenow, J.P. Hartnett, Handbook of Heat Transfer, third ed., McGraw-Hill, New York, 1998.

[53] A.G. Dixon, D.L. Cresswell, Theoretical prediction of effective heat transfer parameters in packed beds, AlChE J. 25 (4) (1979) 663–675.

[54] R. Pesic, T.K. Radoicic, N. Boskovic-Vragolovic, Z. Arsenijevic, Z. Grbavcic, Heat transfer between a packed bed and a larger immersed spherical particle, Int. J. Heat Mass Transf. 78 (2014) 130–136.

[55] N. Wakao, S. Kaguei, Heat and Mass Transfer in Packed Beds, Vol. 1, pp. 243–295, Gorden and Breach, New York, 1982.

[56] F. Kuwahara, M. Shirota, A. Nakayama, A numerical study of interfacial convective heat transfer coefficient in two-energy equation model for convection in porous media, Int. J. Heat Mass Transf. 44 (6) (2001) 1153–1159.

[57] X. Li, Q. Min, X. Wu, S. Liu, Numerical investigation of the flow and temperature uniformly in the reactor core of a pebble bed HTGR using porous media method, in: Proceeding of the 15th International Heat Transfer Conference (IHTC-15, 2014), August 10–15, Kyoto, Japan.

[58] I. Dincer, C. Zamfirescu, Advanced Power Generation Systems, first ed., Elsevier, Amsterdam, 2014.

[59] S.Y. Wu, Y. Chen, Y.R. Li, D.L. Zeng, Exergy transfer characteristics of forced convective heat transfer through a duct with constant wall heat flux, Energy 32 (5) (2007) 686–696.

[60] V. Zimparov, Extended performance evaluation criteria for enhanced heat transfer surface: heat transfer through ducts with constant heat flux, Int. J. Heat Mass Transf. 44 (1) (2001) 169–180.

[61] S. Ergun, Fluid flow through packed columns, Chem. Eng. Prog. 48 (2) (1952) 89–94.

[62] K. Vafai, A. Bejan, W.J. Minkowycz, K. Khanafer, A critical synthesis of pertinent models for turbulent transport through porous media, Advances in Numerical Heat Transfer, Vol. 2, Chapter 12, pp. 389–416, John Wiley & Sons Inc., Hoboken, New Jersey, 2006.

[63] J.S. Lee, K. Ogawa, Pressure drop through packed bed, J. Chem. Eng. Jpn 27 (5) (1994) 691–693.

[64] S. Whitaker, Forced convection heat transfer correlations for flow in pipes, past flat plates, single cylinders, single spheres, and for flow in packed beds and tube bundles, AIChE J. 18 (2) (1972) 361–371.

[65] W.M. Kays, A.L. London, Compact Heat Exchangers, third ed., McGrow-Hill, New York, 1984.

[66] E.C. Nsofor, G.A. Adebiyi, Measurements of the gas-particle convective heat transfer coefficient in a packed bed for high-temperature energy storage, Exp. Thermal Fluid Sci. 24 (1) (2001) 1–9.

[67] F.P. Incropera, D.P. DeWitt, Introduction to Heat Transfer, second ed., John Wiley and Sons Inc., New York, 1990.

[68] R.B. Bird, W.E. Stewart, E.N. Lightfoot, Transport Phenomena, first ed., John Wiley and Sons Inc., New York, 1960.

[69] S.J. Kline, F. McClintock, Describing uncertainties in single-sample experiment, Mech. Eng. 75 (1953) 3–8.

[70] R.J. Moffat, Describing the uncertainties in experimental results, Exp. Thermal Fluid Sci. 1 (1) (1988) 3–17.

[71] H.W. Coleman, W.G. Steele, Experimentation, Validation, and Uncertainty Analysis for Engineers, third ed., John Wiley and Sons Inc., Hoboken, New Jersey, 2009.